

The Vane Angle Influence on the Flow Pattern around a Circular Pier

Tahseen Ali Jabbar¹, Rafi M. Qasim², Bassam A. Mohammed³




¹Department of Fuel and Energy, Southern Technical University, Basra, Iraq (tahseen.ali@stu.edu.iq) ORCID 0000-0002-0602-9627; ²Department of Fuel and Energy, Southern Technical University, Basra, Iraq (rafi.mohammed@stu.edu.iq) ORCID 0000-0002-1882-0766; ³Department of Thermal Mechanical Engineering, Southern Technical University, Basra, Iraq (bassam.moh@stu.edu.iq) ORCID 0000-0003-1647-9645

Abstract

This paper intends to numerically analyze the hydrodynamic characteristics of the flow pattern that surrounds the circular pier near the vane angle. These include flow velocity, turbulent intensity, and pressure. A computational fluid dynamic is proposed to simulate the two-dimensional model by using the finite volume method, while the $k - \epsilon$ turbulence model is used to describe the turbulent model. The vane is located upstream of the pier, with its dimensions as function of the pier diameter. The distance between the vane and the pier center is equal to the pier diameter, the angle of the vane is put with a range from 60° to 180°, and the pier diameter is equal to 10 mm. The turbulent flow has a Reynolds number that varies from 20000 to 50000. The existence of the vane angle leads to two different processes, which are flow separation and flow dissipation, which have a direct effect on flow velocity, turbulent intensity, and pressure. From the current numerical results, the relationships between Reynolds number and average flow velocity, maximum flow velocity, turbulent intensity, and maximum turbulent intensity are more sensitive to flow separation and flow dissipation along the vane. Also, positive and negative pressure distributions have a higher influence on flow separation and flow dissipation.

Author Keywords. Circular Pier. Flow Pattern. Open Channel Flow. Vane Angle.

Type: Research Article

 Open Access  Peer Reviewed  CC BY

1. Introduction

In open channels and rivers, a turbulent flow around circular obstacles (e.g., piers, piles, and pipes) represents a significant problem when assessing the hydrodynamic patterns around an obstacle. For example, scour around the bridge pier and pile is an important factor that contributes to bridge hydraulic collapse against the applied hydrodynamic loading. Several papers have examined this problem so satisfactory solutions could be identified to prevent any hydraulic problems from affecting the structure–flow field interaction. Qasim and Jabbar (2021) numerically analyzed the hydraulic field response that surrounds the cylinder and the neighboring vane when its shape is rectangular. The authors adopted various distances between the vane and the cylinder, leading to results that indicated a dramatic shift in hydraulic response when the vane was directly touching the cylinder. Ramli et al. (2021) used perforated shrouds to dominate the vortex shedding of a circular cylinder. In their study, the Reynolds number was equal to 200 and the shrouds had both uniform and non-uniform holes with a porosity of 67%. The authors used ANSYS Fluent software to analyze all the data. Abdulhussein, Qasim, and Al-Asadi (2019) conducted various experiments to investigate the effect of using special devices to reduce the scour depth around the bridge pier. These

experiments adopted three different pier diameters with three different special devices. According to their results, the use of a special device reduced the scour depth around the pier. [Osrin et al. \(2019\)](#) experimentally investigated the flow pattern past the shrouded cylinder. Their work revealed the impact of perforated shrouds' uniform and non-uniform holes on the cylinder's drag and lift coefficients. They conducted the experiment in a wind tunnel, with the Reynolds number equal to 9.345×10^3 . [Obied and Khassaf \(2019\)](#) examined the impact of using piers containing slots to decrease the scour depth around the bridge pier. The results revealed that scour depth reduction occurred with the increase in the slot's length. [Azmi, Jamil, and Zhou \(2018\)](#) computationally studied the effect of using perforated shrouds to manipulate the unsteady wake behind the circular cylinder. The shrouds had a uniform and non-uniform holes with a porosity of 33% and the computation was done with a Reynolds number equal to 300. The authors were able to determine the impact of the perforated cylinders' hole uniformity on the vortex shedding behind the circular cylinder.

[Abdulhussein and Qasim \(2018\)](#) used some results of previous research to numerically derive three equations, so the scour depth around a cylinder pier could be predicted with the dependency of the flow field characteristics, soil diameter, and pier diameter. [Khassaf and Obied \(2018\)](#) conducted experimental work to reduce the local scour around the bridge pier by using guide panels. The results showed that the depth of the scour around the pier reduced with the reduction of the panel's height. [Gozmen and Akilli \(2014\)](#) used a particle image velocimetry technique to investigate the flow field around a circular cylinder surrounded by an outer permeable cylinder. The study used five different diameters for the outer cylinder with eight different porosities, while a fixed diameter of the inner cylinder was equal to 30 mm. [Tian et al. \(2013\)](#) studied the flow pattern around a cylinder with a rectangular shape, considering different aspect ratios and adopting the two-dimensional unsteady Reynolds-Average Navier-Stokes equation with the $k - \epsilon$ shear stress transport turbulence model. The aspect ratio varied from 0.05 to 1, and the Reynolds number was equal to 21400. The main target of this study was to assess the validity of unsteady Reynolds-Average Navier-Stokes equation with the $k - \epsilon$ shear stress transport turbulence model. [Singha and Sinhamahapatra \(2010\)](#) numerically investigated the flow past a circular cylinder placed centrally inside a channel. The blockage rate was modified with the change in the distance between the walls of the channel. The simulations were performed with a range of Reynolds numbers, which are consistent with the two-dimensional assumption. [Parnaudeau et al. \(2008\)](#) made a numerical and experimental analysis of the flow over a circular cylinder with the Reynolds number equal to 3900. Large eddy simulation was employed to perform numerical analysis, and particle image velocimetry was used to do the experimental work. Also, the work included turbulence statistics and the power spectra in the near wake. [Benim et al. \(2007\)](#) employed the shear stress transport model to numerically study the turbulent flow passing the circular cylinder, with the Reynolds numbers varying from 10^4 to 5×10^6 . [Ali and Karim \(2002\)](#) used Fluent Computational Fluid Dynamics (CFD) to predict the flow pattern around a circular cylinder in three dimensions. The numerical results were adopted to find the variation of the bed shear stress around the cylinder. [Breuer \(1998\)](#) used a large eddy simulation to numerically analyze the turbulent flow passing a circular cylinder with a Reynolds number equal to 3900. The numerical study concentrated on the modeling aspects that are reflected in the quality of the large eddy simulation solution. [Blackburn \(1994\)](#) performed experimental studies to discern the influence of tunnel blockage on the spanwise correlation of the wake of a circular cylinder with the Reynolds number ranging between 2400 and 4000.

The main goal of this present work is to study the reduction of the turbulent flow intensity and flow velocity around the pier by installing a vane angle at upstream of the pier. This vane works as a protection structure that defends the pier against high turbulent flow. The numerical analysis was performed to evaluate the hydrodynamic field around the circular pier. The study provides a reasonable proposition for the vane angle shape design, leading to protection against severe turbulent intensity. Furthermore, it promotes an improved understanding of turbulence around the pier reduction methods.

2. Numerical Modelling

The computational analysis is performed with ANSYS software, which uses the finite volume method and the $k - \epsilon$ turbulent model to perform the study. In the pre-processing step, the two dimensions domains' geometry is sketched, as illustrated in Figure 1, with the cylinder pier diameter equal to 10mm. Meanwhile, the dimensions of the angle vane are set as a function of the pier diameter, and the vane angle ranges between 60° to 180° , with an angle incremental step of 10° . The spacing between the vane and the pier is equal to pier diameter, while the dimensions of the domain are measured from the pier center to the inlet, outlet, and both sides. The inlet and outlet boundaries are both located at $10D$ and $20D$ from the pier center, respectively, while the side's boundaries are both located at $5D$ from the pier center, where D is referred to the pier diameter. Figure 1 shows the boundaries and dimensions of the problem's geometry.

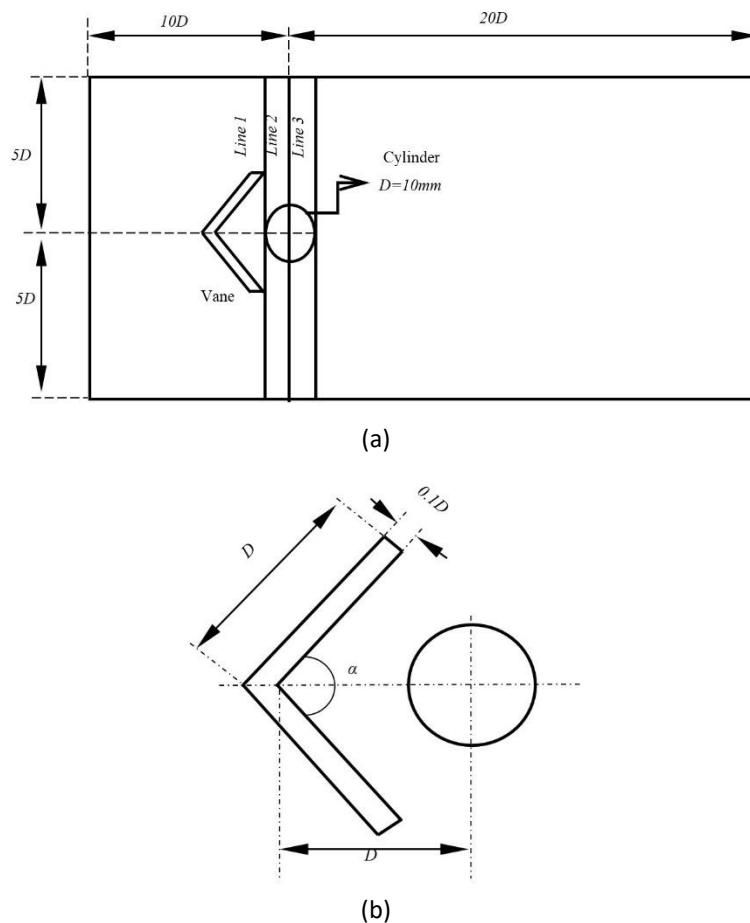


Figure 1: Hydraulic system components with hydraulic domain a) full domain b) the vane and cylinder

Table 1 outlines the boundary conditions adopted during the computational fluid analysis of the present problem. Water is considered the flow material along the channel, as it is

considered an incompressible liquid with constant physical properties and two-dimensional flow analysis. Table 2 reviews the physical properties of the water used in the analysis of the present problem. The different Reynolds numbers used in the analysis varied from 20000 to 50000, while the time used to perform the analysis was 16 seconds. The angle vane is located at the upstream region of the cylindrical pier, while the vane angle values range from 60° to 180° with a step of 10°.

Inlet	Velocity at inlet
Outlet	Pressure at outlet
Cylinder	No slip-Wall
Vane	No slip-Wall
Channel bed	No slip-Wall
Channel sides	No slip-Wall
Top surface of flow	Atmospheric Pressure

Table 1: Boundary conditions of the hydraulic system

Density (kg/m ³)	Viscosity (kg/m.s)
998.2	0.001003

Table 2: Water physical properties

The study investigated the hydrodynamic field around three lines, which are:

- 1) Line 1 located upstream of the pier.
- 2) Line 2 located at the mid-point of the pier.
- 3) Line 3 located downstream of the pier.

The main idea of the present work is to study the hydrodynamic field between the angle vane and the cylindrical pier. The hydrodynamic field can be assessed by the following:

- 1) Normalizing the average flow velocity at lines 1, 2 and 3.
- 2) Normalizing the maximum flow velocity at lines 1, 2 and 3.
- 3) Normalizing the average turbulent intensity at lines 1, 2 and 3.
- 4) Normalizing the maximum turbulent intensity at lines 1, 2 and 3.
- 5) Determine the position of extreme flow velocity and turbulent intensity when the Reynolds number is equal to 50000 and the vane angle goes from 60° to 180° with a step size of 10°.

The present study started with a validation of the simulation of the flow around a square cylinder from works by other researchers (Zaid et al. 2019), as shown in Table 3. The main goal of the validation was to ensure that the adopted software used to solve the problem yield suitable and reliable results. The results obtained from the simulation analysis were compared with the previous results found in the reference (Zaid et al. 2019), as shown in Table 4.

D (m)	V (m/s)	H (m)	ρ (kg/m ³)	Re -
1	0.292	2	1.225	20000

Table 3: Information of study from previous research (Zaid et al. 2019)

Reference studies	Reynolds Number	Setup	C_d
Zaid et al. (2019)	20000	Numerical	2.1951
Present study	20000	Numerical	2.15

Table 4: Illustrate the comparison in results

The CFD governing equations that were used for the simulation are the conservation of momentum equation and incompressible fluid continuity equation. They are shown in Equations (1) to (3), respectively.

$$u \frac{\partial u}{\partial x} + v \frac{\partial u}{\partial y} = -\frac{1}{\rho} \frac{\partial P}{\partial x} + \frac{\mu}{\rho} \left(\frac{d^2 u}{dx^2} + \frac{d^2 u}{dy^2} \right) \quad (1)$$

$$u \frac{\partial v}{\partial x} + v \frac{\partial v}{\partial y} = -\frac{1}{\rho} \frac{\partial P}{\partial y} + \frac{\mu}{\rho} \left(\frac{d^2 v}{dx^2} + \frac{d^2 v}{dy^2} \right) \quad (2)$$

$$\frac{\partial(\rho u)}{\partial x} + \frac{\partial(\rho v)}{\partial y} = 0 \quad (3)$$

here u, v, μ, ρ represent the x and y velocity component, viscosity and density, respectively.

The turbulence kinetic energy, k , and its dissipation rate, ε , are calculated from:

$$\frac{Dk}{Dt} = \frac{\partial}{\partial X_i} \left\{ \left(\nu \delta_{jk} + c_s \frac{k}{\varepsilon} \bar{u}_k \bar{u}_j \right) \frac{\partial k}{\partial X_k} \right\} - \bar{u}_k \bar{u}_j \frac{\partial u_i}{\partial X_k} - \varepsilon \quad (4)$$

$$\frac{D\varepsilon}{Dt} = \frac{\partial}{\partial X_i} \left\{ \left(\nu \delta_{jk} + c_1 \frac{k}{\varepsilon} \bar{u}_k \bar{u}_j \right) \frac{\partial \varepsilon}{\partial X_k} \right\} - \frac{\varepsilon}{k} c_2 \bar{u}_k \bar{u}_j \frac{\partial u_i}{\partial X_k} - c_3 \varepsilon \quad (5)$$

Model constants: C_s, C_1, C_2 and C_3 are 0.22, 0.18, 1.44 and 1.92, respectively (Dahkil, Gabbar, and Jaber 2014).

3. Results and Discussion

Figure 2, Figure 3 and Figure 4 show the relationship among normalized average velocity, normalized maximum velocity, normalized turbulent intensity, and normalized maximum turbulent intensity with different Reynolds numbers and different vane angles in different lines. Both Figures 2(a) and 2(b) show the variation of the average flow and maximum flow velocity, respectively, with different Reynolds numbers for a vane angle equal to 60°. It is clear from the figure that with the increase of the Reynolds number, the average flow velocity and the maximum flow velocity gradually increase, regardless of the position of the line with respect to the vane. This happens with a direct proportion between flow velocity and the Reynolds number. Figure 2(c) shows the relationship between the average turbulent intensity and Reynolds number, being visible that as the Reynolds number increases, the turbulent intensity decreases, regardless of the line position. This noticeable trend in behavior depends on alternating flow separation and flow dissipation. The change in the flow separation zone, supported by the dissipation in flow energy along the vane, will have a strong share in reducing the turbulent intensity, regardless of the value of the flow velocity that affects Reynolds number and turbulent intensity. Figure 2(d) shows the relationship between the maximum turbulent intensity and Reynolds number. From this figure, it is possible to consider that this variation has a strong dependence on the line position. The fluctuation in turbulent intensity with the Reynolds number relies on flow separation and flow dissipation. As the Reynolds number increases, the turbulence continues to increase strongly, while the turbulence suffers in fluctuation due to the presence of the angle vane, leading to an interaction between flow separation and flow dissipation. Both Figures 3(a) and 3(b) show the relationship of the average flow and maximum flow velocity, respectively, with different Reynolds numbers, for a vane angle equal to 120°. It is clear from the figures that, as the Reynolds number increases, average flow velocity and maximum flow velocity also increase, regardless of the position of the line with respect to the vane. This happens with a direct proportion between flow velocity

and Reynolds number. However, the highest values of average flow velocity occur at line 2, while the highest values of maximum flow velocity occur at line 3. Figure 3(c) shows the relationship between average turbulent intensity and Reynolds number, and it is visible from the figure that with the increase of Reynolds number, turbulent intensity also increases, regardless of the line position, which happens in all the lines. Figure 3(d) shows the relationship between maximum turbulent intensity and Reynolds number; being clear from the figure that the variation can be considered strong depending on the line position. Figures 4(a), 4(b), 4(c), and 4(d) show changes in the flow velocity, maximum flow velocity, turbulent intensity and maximum turbulent intensity with the Reynolds number, respectively. The reasonable explanation for differences in the hydrodynamic field is associated with the change that occurs in the value of the vane angle. So, when the vane angle changes, the vane configuration is changed accordingly, which is then reflected in the position of the flow separation zone and the magnitude of the dissipated flow energy. So, we infer that the vane angle dominates the hydrodynamic response.

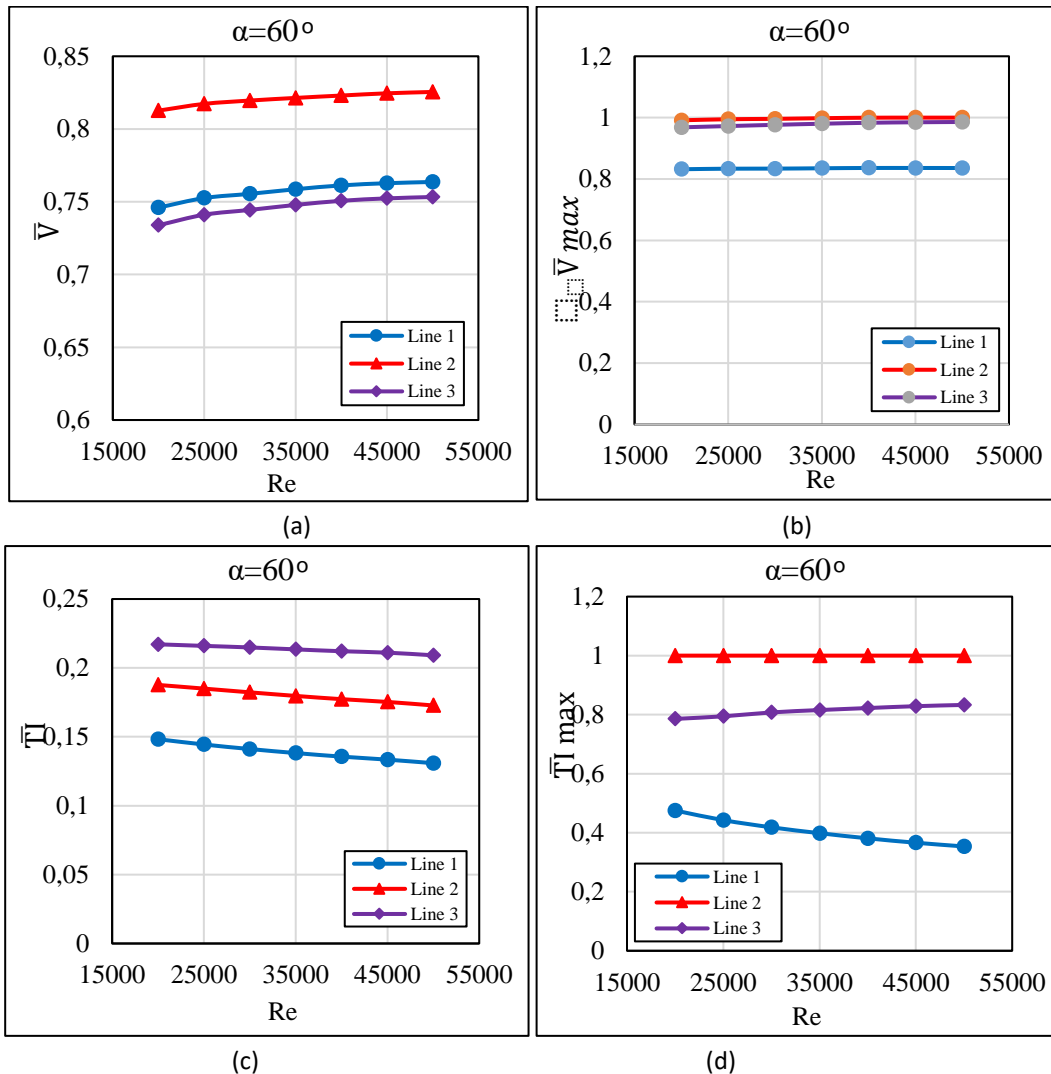


Figure 2: (a) normalized average velocity, (b) normalized maximum velocity, (c) normalized average turbulent intensity, (d) normalized maximum turbulent intensity [at angle (60°)]

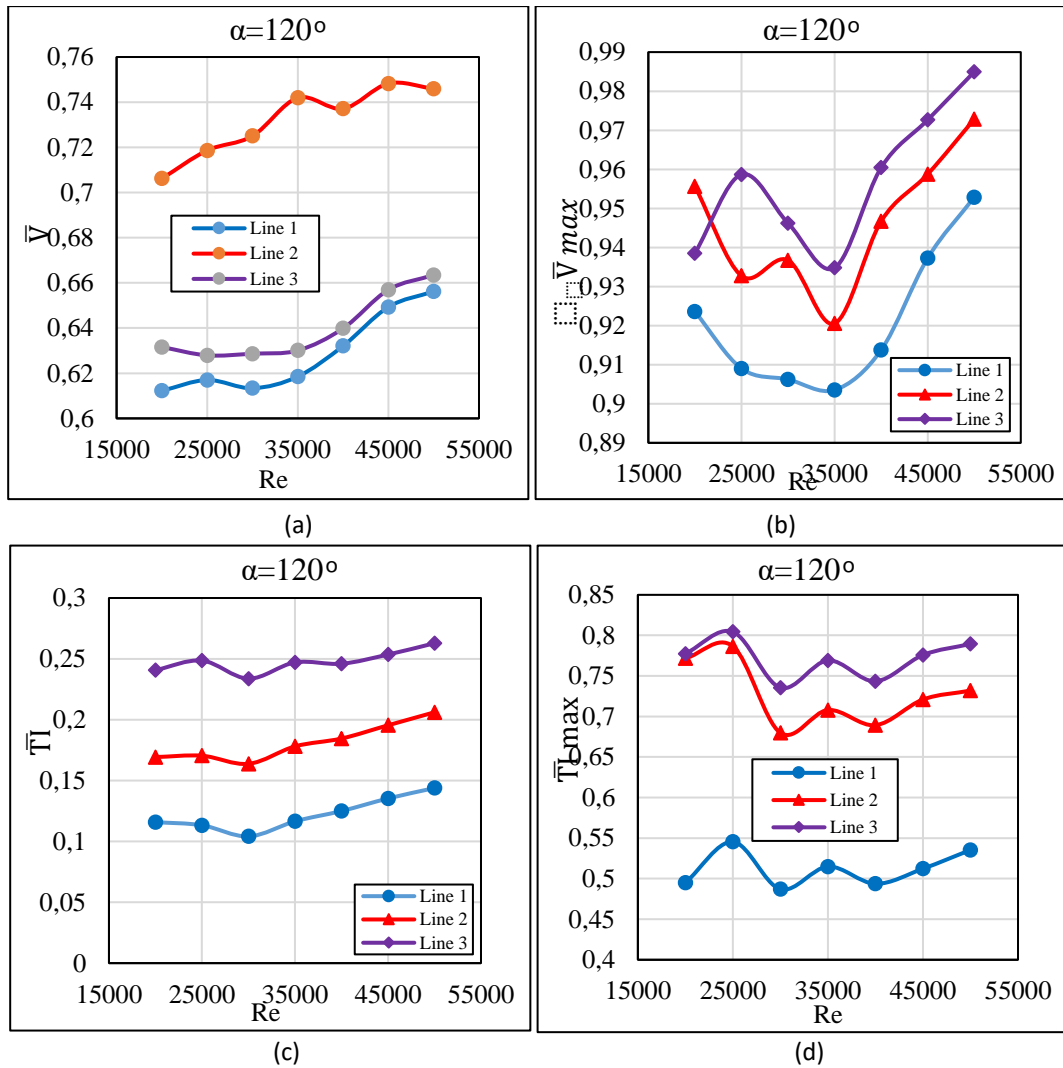


Figure 3: (a) Normalized average velocity, (b) Normalized maximum velocity, (c) Normalized average turbulent intensity, (d) Normalized maximum turbulent intensity [at angle (120°)]

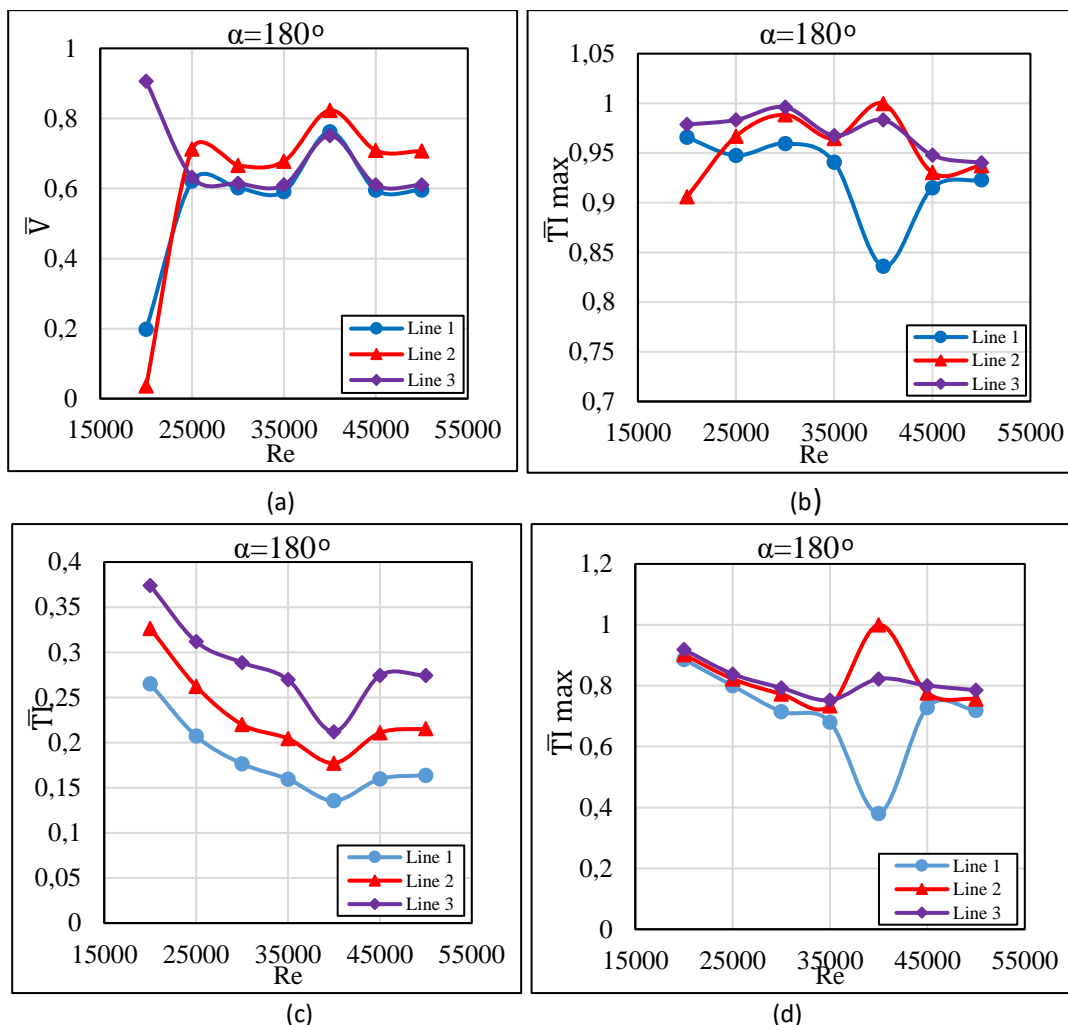
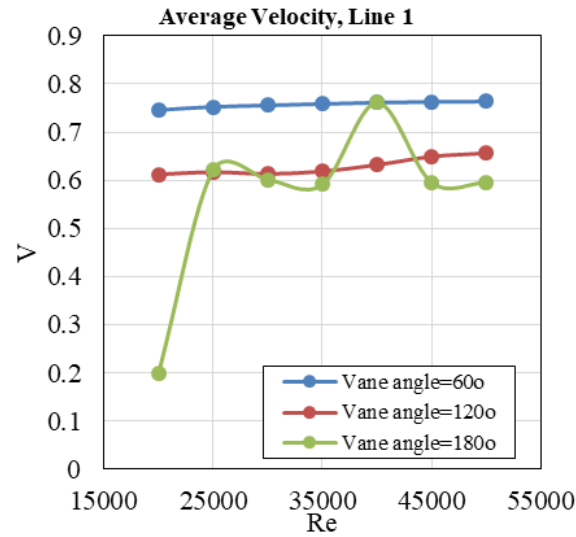
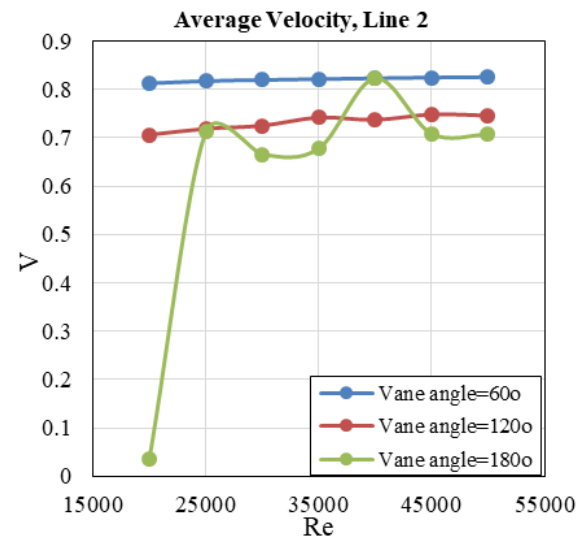


Figure 4: (a) Normalized average velocity, (b) Normalized maximum velocity, (c) Normalized average turbulent intensity, (d) Normalized maximum turbulent intensity [at angle (180°)]

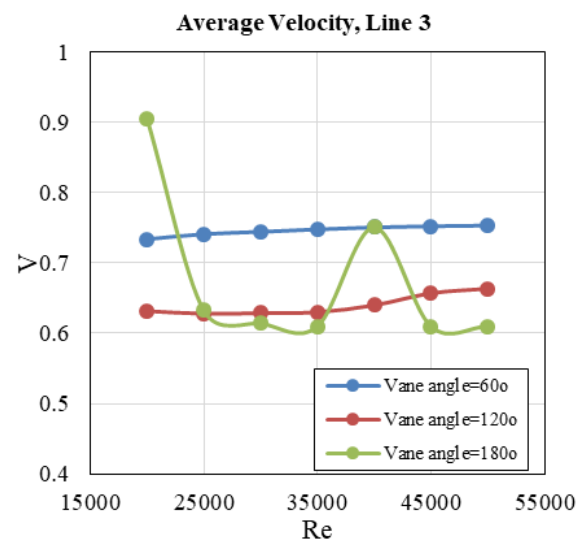
The distribution of the average flow velocity, maximum flow velocity, turbulent intensity and maximum turbulent intensity for a variety of vane angles are presented in Figures 5, 6, 7 and 8, considering the three lines (1, 2 and 3). In Figure 5, the average flow velocity is plotted against the Reynolds number. The figure clearly illustrates a gradual increase in the average flow velocity with the increase of Reynolds number. This increase occurs at lines 1 and line 2, while there is some variation in the relationship trend occurring at line 3 due to the interference between the separation flow process and dissipation flow process. In Figure 6, the maximum flow velocity is plotted against the Reynolds number. It is obvious from the figure that as the Reynolds number increases, the maximum flow velocity also increases at lines 1 and 2, while a dramatic behavior happens at line 3 due to the interference between the separation flow process and dissipation flow process. Figure 7 shows the relationship between turbulent intensity and Reynolds number, and Figure 8 shows the relation between maximum turbulent intensity and Reynolds number. In general, the fluctuation in the obtained results can be attributed to the interference between the separation flow process and dissipation flow process, which depends on the process that occurs first. The change in the position of the flow separation zone has a major effect on turbulent intensity, and the dissipation process leads to reducing the magnitude of flow velocity and will have an effect on the turbulent intensity.



(a)

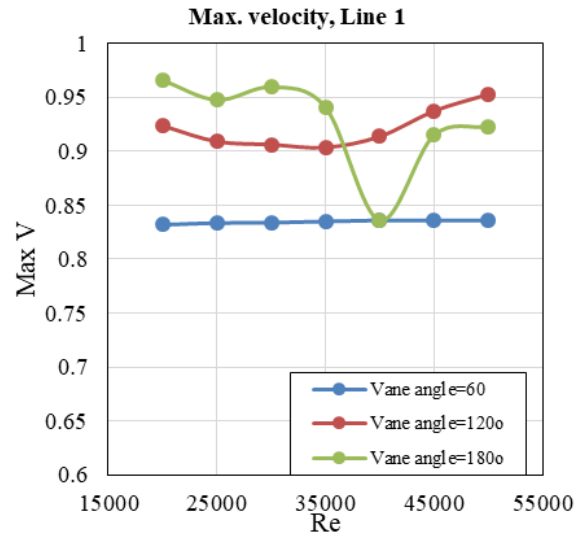


(b)

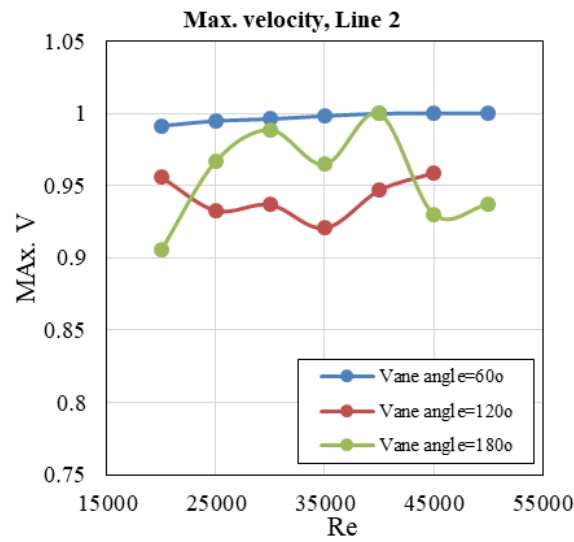


(c)

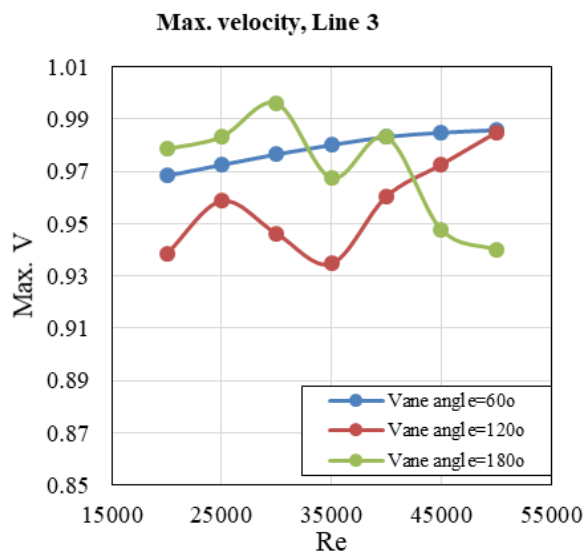
Figure 5: Relation between average flow velocity and Reynolds number for different vane angles



(a)

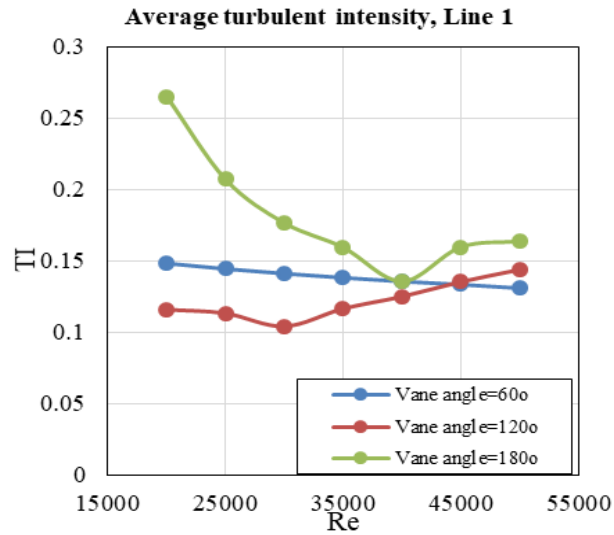


(b)

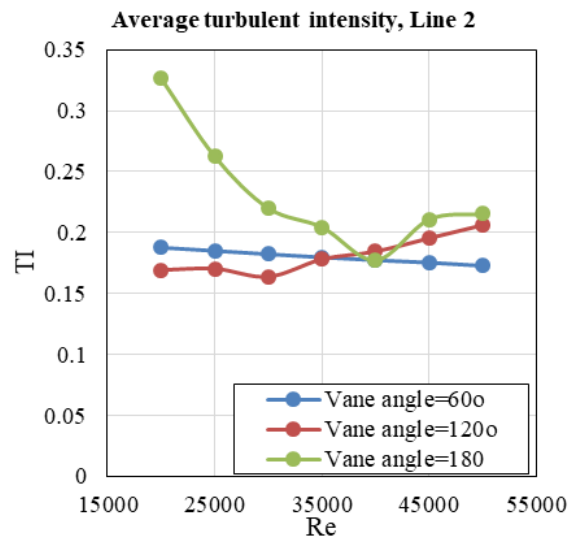


(c)

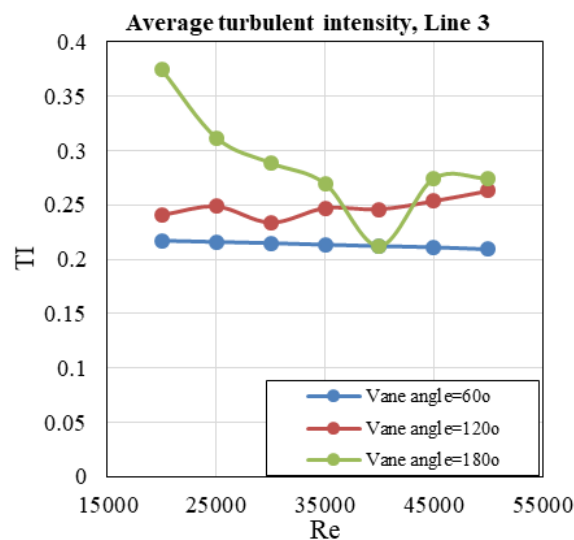
Figure 6: Relation between maximum flow velocity and Reynolds number for different vane angles



(a)

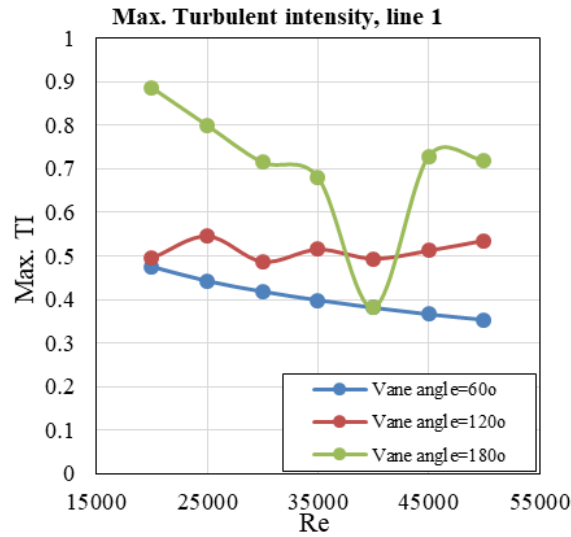


(b)

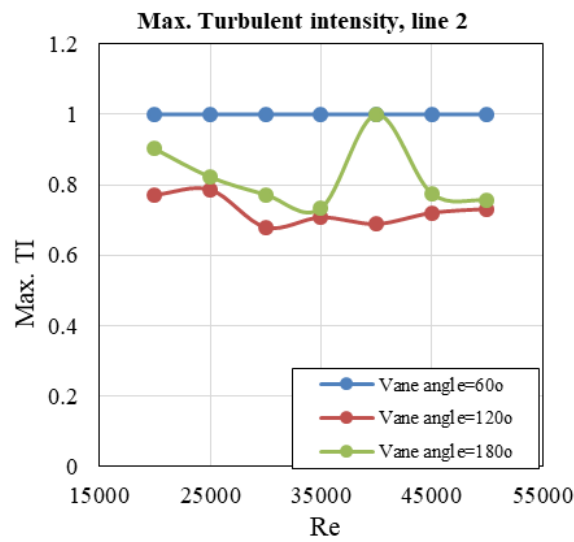


(c)

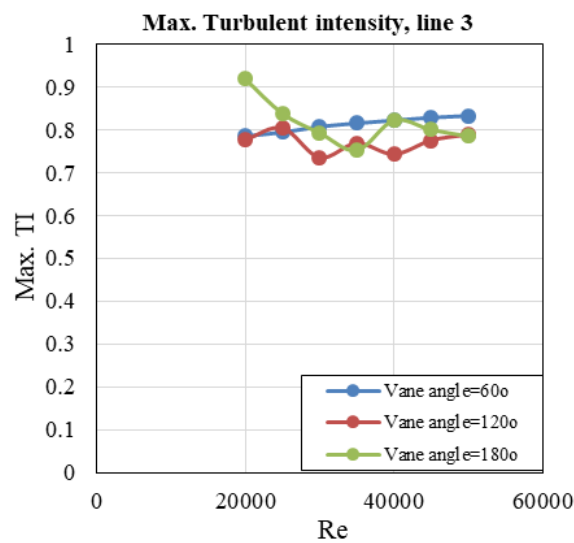
Figure 7: Relation between average turbulent intensity and Reynolds number for different vane angles



(a)



(b)



(c)

Figure 8: Relation between maximum turbulent intensity and Reynolds number for different vane angles

Figure 9 shows the flow velocity contours for various Reynolds numbers. Here, Reynolds numbers range from 2000 to 5000 with a step size equal to 500. We observe from the figure that the flow friction starts from a lower amount at the pier wall downstream and gradually increases with the increase in Reynolds number. A low Reynolds number leads to a low flow velocity due to the direct proportion between the Reynolds number and flow velocity. When the flow velocity is considered low, the flow dissipation at the vane is high when compared to the flow separation at the vane, leading to reduced flow friction that is developed downstream of the pier. This happens when the Reynolds number ranges from 2000 to 2500, while the reverse happens when the Reynolds number is considered high, and the flow separation dominates compared to the flow separation. Therefore, flow friction increases downstream of the pier, which happens when the Reynolds numbers range from 3000 to 5000. Figure 10 shows the maximum flow velocity contours for various Reynolds numbers. Here, Reynolds number ranges from 2000 to 5000 with a step size equal to 500. The variation in the maximum flow velocity depends on the flow separation and flow dissipation. For both Figures 9 and 10, the value of the vane angle is equal to 80° .

Figure 11 shows the turbulent intensity contours for various Reynolds numbers. Here, Reynolds numbers range from 2000 to 5000 with a step size equal to 500. In general, as flow velocity increases, turbulence also increases. In the present study, the presence of the angle vane leads to a decrease in the turbulent intensity due to the reduction of flow velocity. The reduction in flow velocity happens because of the processes of flow separation and dissipation. These processes will directly reflect in the turbulent flow intensity, which clearly is shown in the contours. It is very evident from the figure that as flow velocity increases, eddies and vortices vanish due to the processes of separation and dissipation that control the flow energy. In this study, the value of the vane angle is equal to 80° . Figure 12 shows the pressure contours for various Reynolds numbers. Here, Reynolds numbers range from 2000 to 5000 with a step size equal to 500. It is obvious from the contours that positive pressure occurs upstream of the vane, while negative pressure occurs around and downstream of the cylinder. The presence of the vane upstream of the pier leads to a variation in the pressure. The contours show that both positive and negative pressure increase with an increase of the Reynolds number. The difference in the pressure distribution is attributed to the change in the momentum transfer from section to section. Regarding the mechanism of the vane that is responsible for the distribution of positive and negative pressure, the vane reverses the direction of the flow and works to separate the flow. Therefore, we inferred that as separation increases, flow velocity decreases, which leads to an increase in both positive and negative pressure. Also, the dissipation of flow leads to a reduction in flow velocity and increased positive pressure.

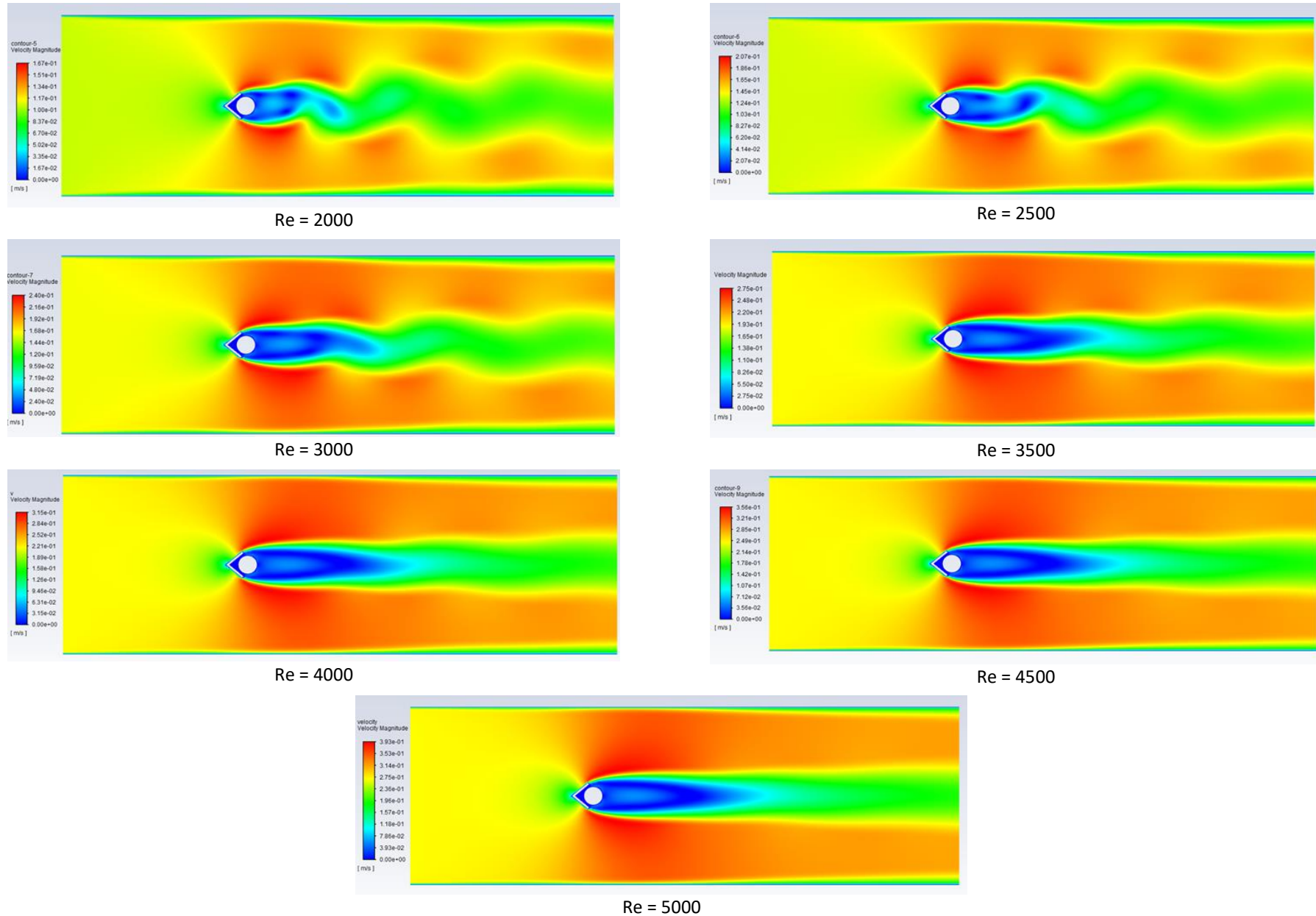


Figure 9: Flow velocity contours for different Reynolds numbers

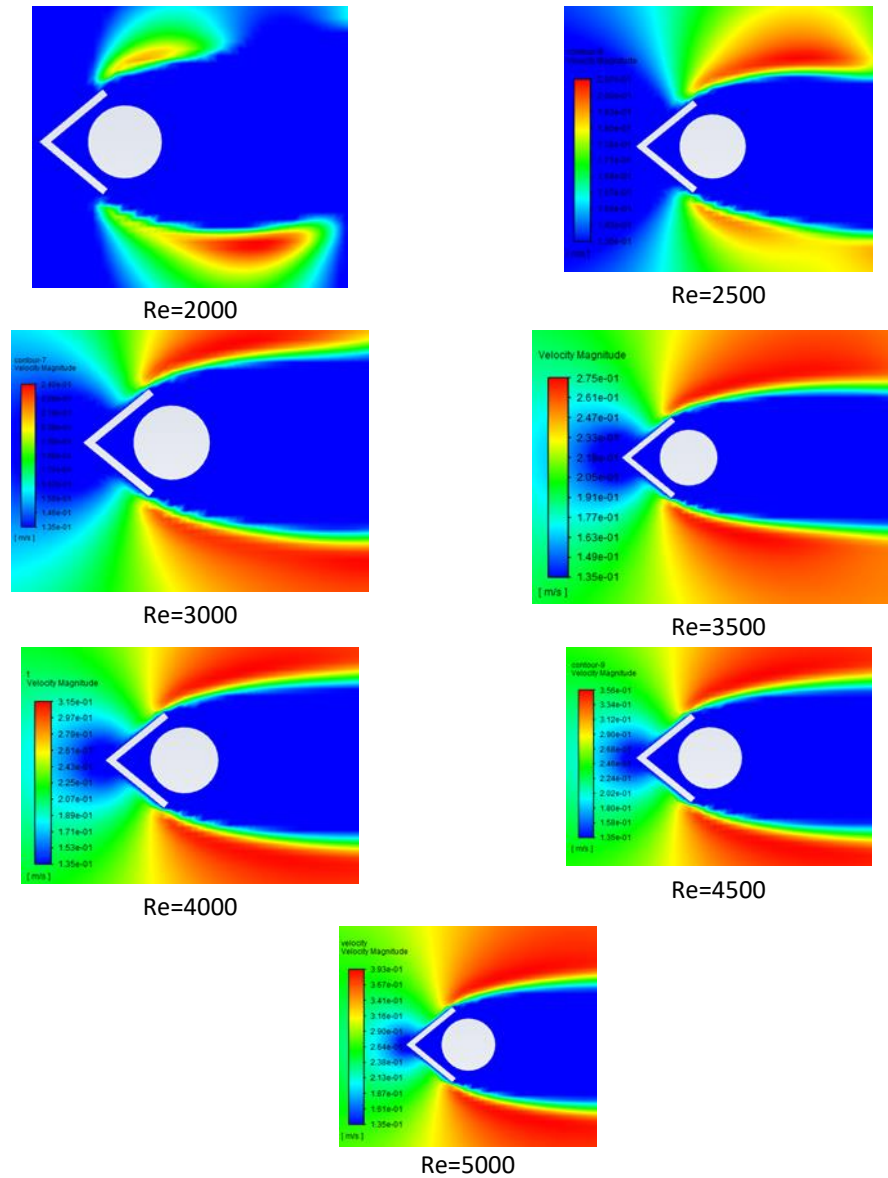


Figure 10: Flow velocity contours for different Reynolds numbers

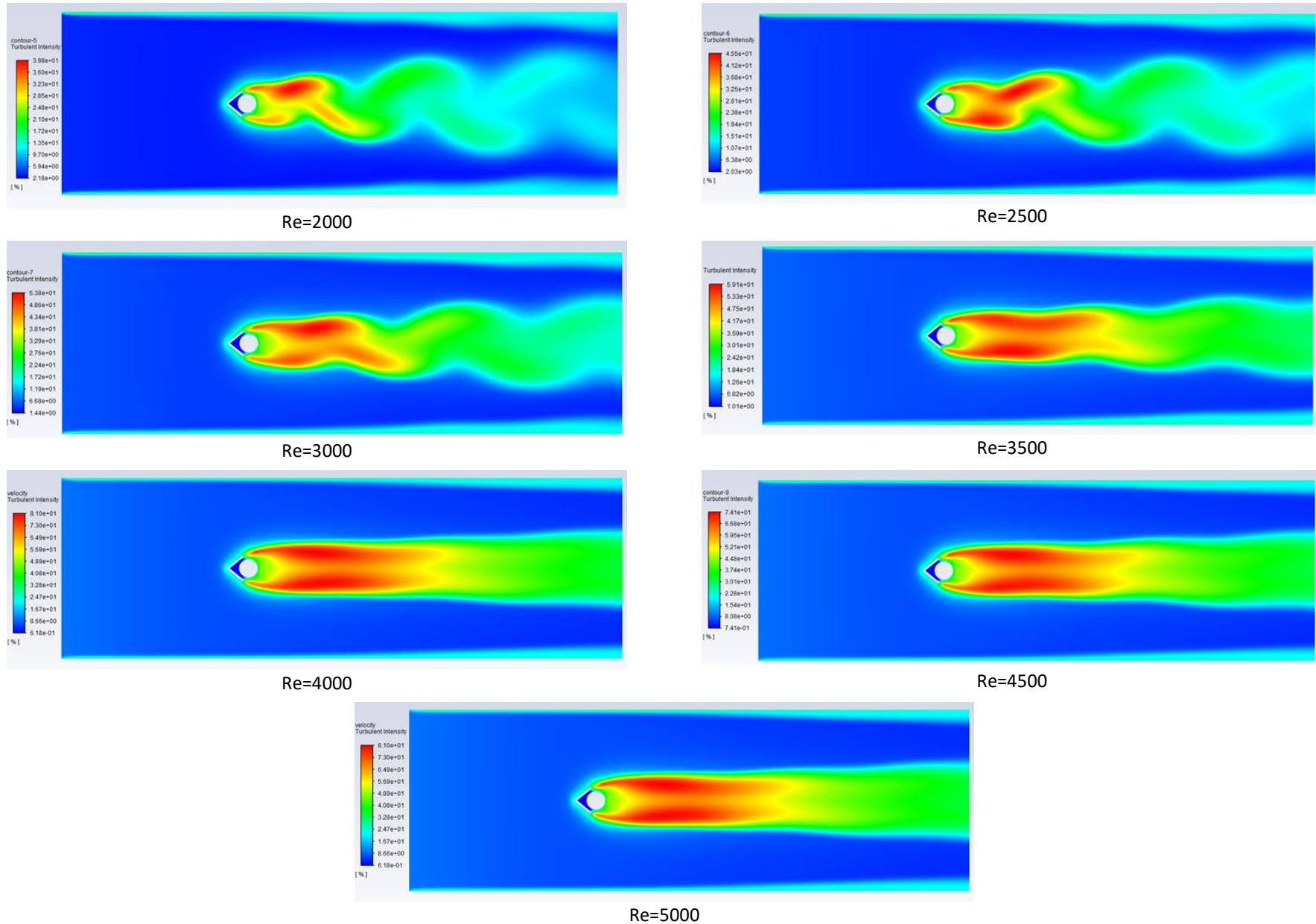


Figure 11: Flow velocity contours for different Reynolds numbers

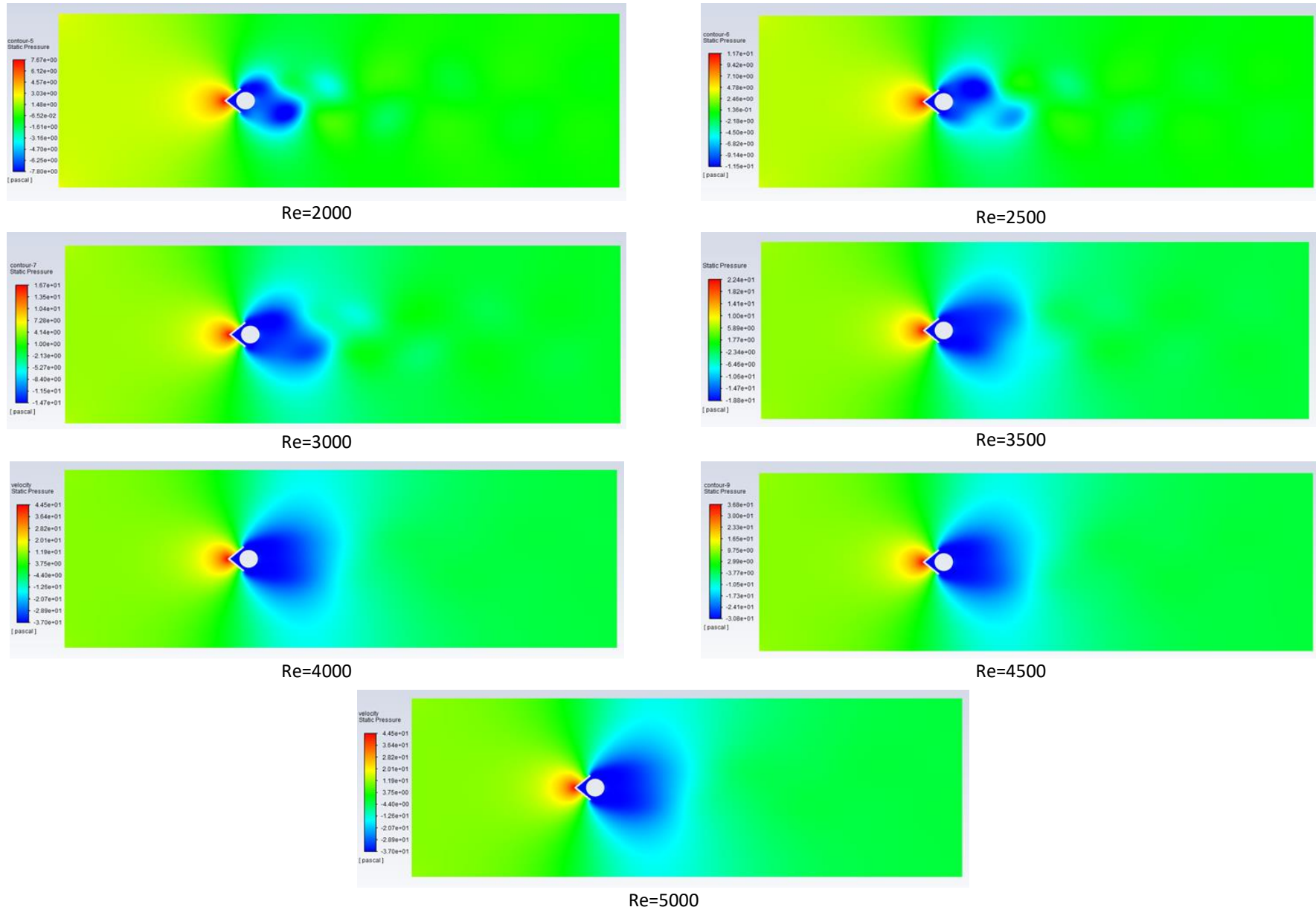


Figure 12: The pressure contour for various Reynolds number

Figure 13 explains how to determine the position of extreme flow velocity and extreme turbulent intensity in terms of the coordinates (x,y). Figure 14 and Figure 15 show the variation of the x-coordinate and y-coordinate of the flow velocity, respectively, in terms of the vane angle. Also, Figure 16 and Figure 17 show the x-coordinate and y-coordinate of the turbulent intensity, respectively, in terms of the vane angle. The change in the position of the extreme point depends on different variables, like the flow velocity, flow separation zone, and energy dissipation. These figures are drawn to cover the entire range of the vane angle where the adopted Reynolds number is equal to 50000.

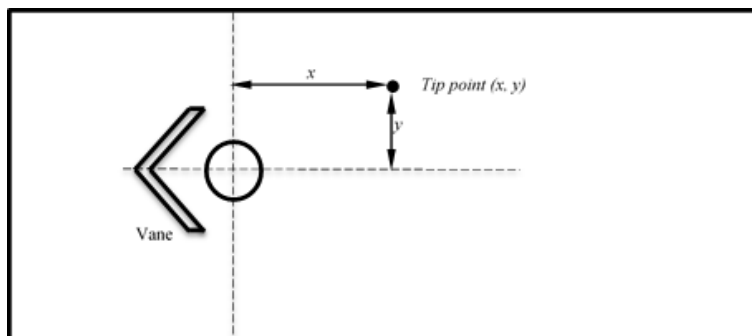


Figure 13: Location of the extreme point

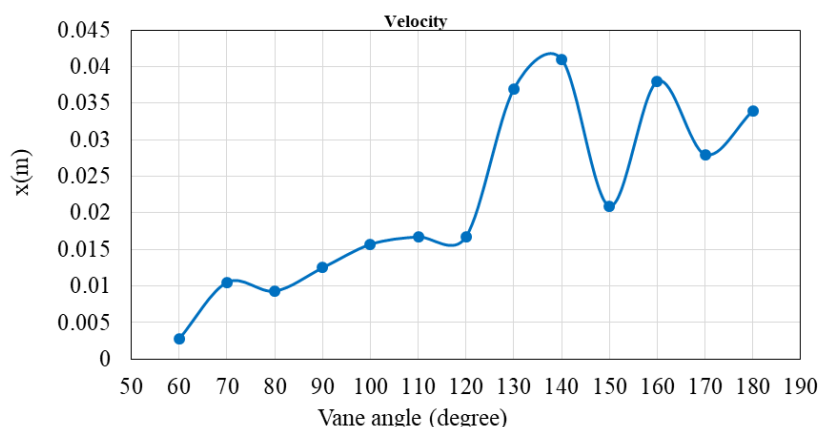


Figure 14: Variation in the x-coordinate of the flow velocity in terms of the vane angle (Re=50000)

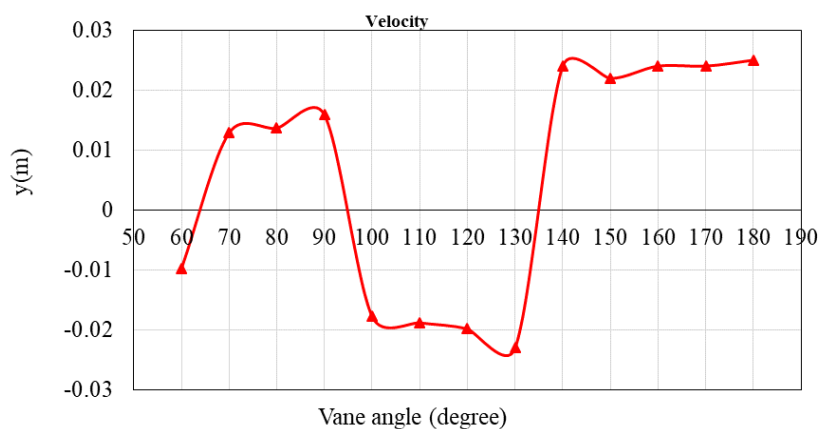


Figure 15: Variation in the y-coordinate of the flow velocity in terms of the vane angle (Re=50000)

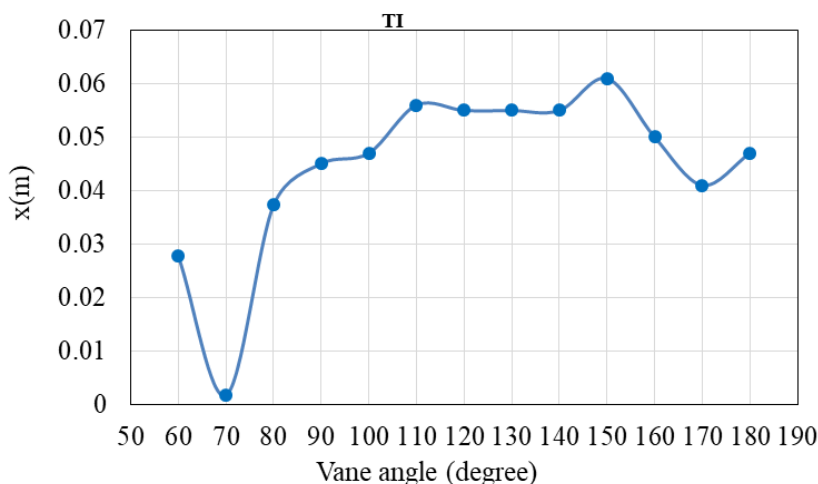


Figure 16: Variation in the x-coordinate of the turbulent intensity in terms of the vane angle (Re=50000)

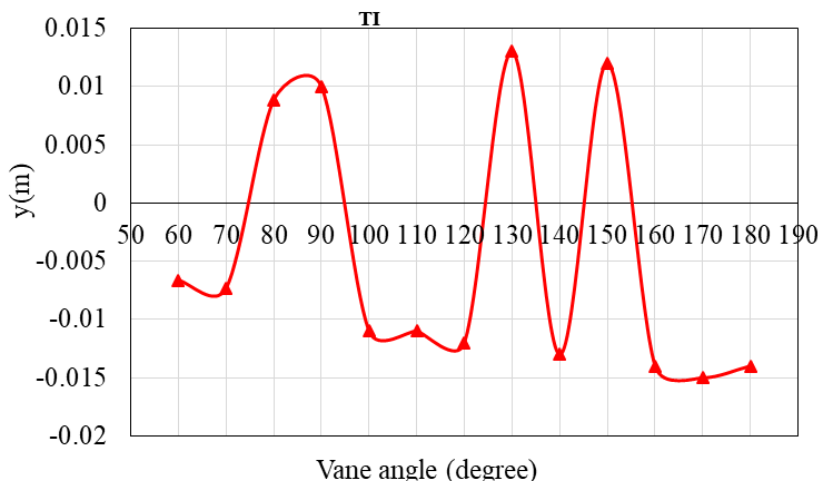


Figure 17: Variation in the y-coordinate of the turbulent intensity in terms of the vane angle (Re=50000)

4. Conclusions

Numerical studies of the flow around a cylinder pier have been performed by using CFD under a vane angle varying from 60° to 180°. The variation in the hydrodynamic field is expressed in terms of flow velocity and turbulent intensity. This study has found that flow separation and flow dissipation are controlled by the hydrodynamic field, and the results also show that a Reynolds number with a low value is more sensitive to the flow dissipation processes, whereas one with a high value is more sensitive to the flow separation processes. In addition, any variation in the flow velocity is reflected directly in the flow turbulent intensity. Changes in the values of the vane angle have an effect on the magnitude and position of the average flow velocity, maximum flow velocity, turbulent intensity, and maximum turbulent intensity. Furthermore, changes in the values of maximum flow velocity, average flow velocity, maximum turbulent intensity, and turbulent intensity depend mainly on flow separation and flow dissipation. The presence of the vane leads to a change in the pressure distribution around a cylinder pier. The value and location of positive and negative pressure depend mainly on flow dissipation and flow separation. A contour map of the flow velocity, maximum flow velocity, and turbulent intensity gives a good idea of eddies formation and dissipation depending on flow velocity.

References

- Abdulhussein, I. A., and R. M. Qasim. 2018. "Determination of local scour depth of prototype cylindrical pier using physical model data collection". *International Journal of Civil Engineering and Technology* 9, no. 9: 1283-301.
- Abdulhussein, I. A., R. M. Qasim, and K. Al-Asadi. 2019. "Pier scouring reduction using a Strip Guide Flow Panel device". *RUDN Journal of Engineering Research* 20, no. 3: 229-35. <https://doi.org/10.22363/2312-8143-2019-20-3-229-235>.
- Ali, K. H. M., and O. Karim. 2002. "Simulation of flow around piers". *Journal of Hydraulic Research* 40, no. 2: 161-74. <https://doi.org/10.1080/00221680209499859>.
- Azmi, A. M., H. Jamil, and T. Zhou. 2018. "Effect of hole-uniformity of shrouds on vortex shedding suppression behind a circular cylinder". *IOP Conference Series: Materials Science and Engineering* 417: 012036. <https://doi.org/10.1088/1757-899X/417/1/012036>.
- Benim, A. C., M. Cagan, A. Nahavandi, and E. Pasqualotto. 2007. "RANS predictions of turbulent flow past a circular cylinder over the critical regime". In *Proceedings of the 5th IASME / WSEAS International Conference on Fluid Mechanics and Aerodynamics*, 235-40. WSEAS Press.
- Blackburn, H. M. 1994. "Effect of blockage on spanwise correlation in a circular cylinder wake". *Experiments in Fluids* 18, no. 1-2: 134-36. <https://doi.org/10.1007/BF00209371>.
- Breuer, M. 1998. "Numerical and modeling influences on large eddy simulations for the flow past a circular cylinder". *International Journal of Heat and Fluid Flow* 19, no. 5: 512-21. [https://doi.org/10.1016/S0142-727X\(98\)10015-2](https://doi.org/10.1016/S0142-727X(98)10015-2).
- Dahkil, S. F., T. A. Gabbar, and D. K. Jaber. 2014. "Numerical study of the initial pressure and diameters ratio effect on the jet ejector performance". *Basrah Journal for Engineering Science* 14, no. 1: 122-35. <https://www.iasj.net/iasj/article/93851>.
- Gozmen, B., and H. Akilli. 2014. "Flow control downstream of a circular cylinder by a permeable cylinder in deep water". *Wind and Structures, An International Journal* 19, no. 4: 389-404. <https://doi.org/10.12989/was.2014.19.4.389>.
- Khassaf, S. I., and N. A. Obied. 2018. "Experimental study: Bridge pier protection against local scour using guide panels". *IOP Conference Series: Materials Science and Engineering* 433: Article number 012006. <https://doi.org/10.1088/1757-899X/433/1/012006>.
- Obied, N. A., and S. I. Khassaf. 2019. "Experimental study for protection of piers against local scour using slots". *International Journal of Engineering, Transactions B: Applications* 32, no. 2: 284-91. <https://doi.org/10.5829/ije.2019.32.02b.05>.
- Osrin, M. F., A. M. Azmi, H. Yusoff, and N. A. Razak. 2019. "Effect of shroud hole on the force characteristics of a circular cylinder". *International Journal of Engineering and Advanced Technology* 9, no. 1: 5929-35. <https://doi.org/10.35940/ijeat.A3030.109119>.
- Parnaudeau, P., J. Carrier, D. Heitz, and E. Lamballais. 2008. "Experimental and numerical studies of the flow over a circular cylinder at Reynolds number 3900". *Physics of Fluids* 20, no. 8: Article number 085101. <https://doi.org/10.1063/1.2957018>.
- Qasim, R. M., and T. A. Jabbar. 2021. "An analytic study of the effect of a vane on the hydraulic field around a cylinder". *INCAS Bulletin* 13, no. 3: 123-39. <https://doi.org/10.13111/2066-8201.2021.13.3.11>.
- Ramli, N. A., A. M. Azmi, A. H. A. Hamid, Z. A. K. Baharin, and T. Zhou. 2021. "Effect of cylinder gap ratio on the wake of a circular cylinder enclosed by various perforated shrouds". *CFD Letters* 13, no. 4: 51-68. <https://doi.org/10.37934/cfdl.13.4.5168>.

- Singha, S., and K. P. Sinhamahapatra. 2010. "Flow past a circular cylinder between parallel walls at low Reynolds numbers". *Ocean Engineering* 37, no. 8-9: 757-69. <https://doi.org/10.1016/j.oceaneng.2010.02.012>.
- Tian, X., M. C. Ong, J. Yang, and D. Myrhaug. 2013. "Unsteady RANS simulations of flow around rectangular cylinders with different aspect ratios". *Ocean Engineering* 58: 208-16. <https://doi.org/10.1016/j.oceaneng.2012.10.013>.
- Zaid, M., Z. Yazdanfar, H. Chowdhury, and F. Alam. 2019. "Numerical modeling of flow around a pier mounted in a flat and fixed bed". *Energy Procedia* 160: 51-59. <https://doi.org/10.1016/j.egypro.2019.02.118>.